scientific reports

Check for updates

OPEN

Analysis of the color-oversaturation problem in WCGDs and promising EOTF-based solution strategies

Fengxia Liu[1,2], Xifeng Zheng[1,2,3], Junchang Chen[1,2], Deju Huang[1,2,4], Jingxu Li[1,2,4], Yu Chen[1,2,3,4], Yang Wang[1,2,3,4], Hui Cao[3,4], Zicheng Xu[1,2,4], Yufeng Chen[1,2,3,4] & Xinyue Mao[1,3]✉

The gamut and EOTF (Electro-Optical Transfer Function) of a display together determine its color performance. Gamut determines the range of displayable colors, and the EOTF determines the color accuracy and depth. Image reproduction often comprises two parts: the image source and the display terminal. To ensure the universality of different terminals, the image source is generally produced in a standardized gamut standard, while the terminal pursues a wider gamut and more spectacular color performance. As a widely welcomed form of display, WCGDs (Wide Color Gamut Displays) boast stunning color performance. However, certain colors in WCGDs displays are oversaturated, which is unacceptable to the human eye. This paper analyzes the oversaturation problem of WCGDs. Firstly, a display model based on EOTF and gamut parameters is established. Then the color point vector field varies with EOTF is derived and the drift of luminance and chromaticity are analyzed separately. Finally, two strategies are present to optimize the color oversaturation problem of WCGDs based on the analysis conclusions and verify its effectiveness. This paper presents a detailed analysis and possible strategy for color oversaturation in WCGDs, providing a theoretical basis for the accurate color reproduction and efficient color management of WCGDs.

Gamut refers to the upper limit of the display's color reproduction capability[1]. The display gamut has undergone an evolution from black-white displays to WCGDs[2]. The emergence of colored displays made it possible to present an abundance of colors, but the gamut was limited and differed tremendously from one display to another[3]. With the formulation and promotion of the sRGB gamut standard, the display gamut was gradually standardized, thus the accuracy and consistency of color reproduction were greatly promoted[4]. Nowadays, WCGDs are becoming mainstream, capable of a wider gamut coverage, such as Adobe RGB, DCI-P3, BT2020, etc., which can provide a more abundant visual experience for application scenarios such as images, videos, and games[5]. With the widespread application of HDR technology in recent years, the color reproduction of displays has been further enhanced, with significant improvement in color accuracy and depth, and more vivid and realistic colors[6]. The evolution of gamut not only enhances the user experience but also promotes the growth of image and video content creation such as photography, film and television production, image processing, etc, and facilitates the development and innovation of color management and display technology, bringing new possibilities for visual presentation in the digital era.

WCGDs can present more vibrant and saturated colors, yet this vibrancy and saturation are often inconsistent with the actual perception of the human eye, resulting in the problem of color oversaturation, especially blue sky, grass, skin color, and other memory colors known to humans[7,8]. Color oversaturation significantly affects the realism of image reproduction and makes the viewing experience much less pleasant. Therefore, when designing and using WCGDs, special attention must be paid to color accuracy and balance to attenuate color distortion issues and provide a superior visual experience[9].

This paper first briefly introduces the imaging mechanism of WCGDs and analyzes the possible reason for color oversaturation. Then combined with the basic color model of the display, we thoroughly examine the influence of the EOTF curve on display color reproduction, mainly the variation of the color parameters with the mathematical characteristics of EOTF, including the luminance and chromaticity deviations. On this basis, a color oversaturation solution based on the EOTF curve is proposed in conjunction with the display

[1]Fine Mechanics and Physics, Chinese Academy of Science, Changchun 130013, Jilin, China. [2]University of Chinese Academy of Sciences, Beijing 100049, China. [3]Cedar Electronics Changchun (Technology Co., Ltd), Changchun 130013, Jilin, China. [4]These authors contributed equally: Jingxu Li, Yu Chen, Yang Wang, Hui Cao, Zicheng Xu and Yufeng Chen. ✉email: maoxy@ccxida.com

characteristics of WCGDs, and its feasibility and validity are verified according to a color difference index in uniform color space at the end.

WCGDs and color oversaturation problems

The display imaging process consists of two parts: the image source and the display terminal, as shown in Fig. 1. The image source is captured in some form of OOTF (Optical Optical Transfer Function) and then encoded by inverse EOTF for photoelectric conversion and output as an image file of a certain color standard. The image source is input to the display system and then decoded by the display system EOTF into an optical signal for display[10].

For the image source, to ensure the universality among different devices, image files are usually demanded to be produced in a standard gamut. Different color gamut standards have been developed for different application scenarios, such as sRGB for universal[4], Adobe RGB for professional display[11], BT2020 for HDTV[12], DCI-P3 for cinema[13], etc., respectively corresponding to different coding manners and storage formats. The image source of the sRGB standard is typically stored in 8bit, corresponding to 65,535 colors, and its EOTF function is usually an exponential function with a power of 2.2, Adobe RGB is generally stored in 12bit, corresponding to 68 billion colors, and its EOTF is usually an exponential function with a power of 2.2, while DCI-P3 is typically required the image source to meet the 16bit HDR standard with PQ curve[14].

For the display, limited by LEDs characteristics and control system capabilities, the display terminal generally has a maximum gamut border and minimum control accuracy[15]. It is often expected to fully utilize the gamut advantages and control capabilities of the display system to pursue better visual effects[16]. In our previous work, we have established the basic display model of the display terminal as follows Eqs. (1)–(3)[17].

$$[X \quad Y \quad Z]^T = H\,[eotf\,(r) \quad eotf\,(g) \quad eotf\,(b)]^T \tag{1}$$

$$x = \frac{X}{X+Y+Z} \tag{2}$$

$$y = \frac{X}{X+Y+Z} \tag{3}$$

where r, g, b are uncoded linear color component values, range for [0,1].

$eotf(x)$ is the EOTF of the display system, the input signal is encoded by the EOTF and the output is a nonlinear color component, usually in terms of the actual display luminance, and normalized values are used throughout this paper.

H is the display characterization matrix of the display, determined by the LEDs chromatic parameters (x_*, y_*, z_*) and the white balance ratio C_1, C_2, C_3, it is denoted as[18]:

$$H = \begin{bmatrix} C_1\frac{x_r}{y_r} & C_2\frac{x_g}{y_g} & C_3\frac{x_b}{y_b} \\ C_1 & C_2 & C_3 \\ C_1\frac{z_r}{y_r} & C_2\frac{z_g}{y_g} & C_3\frac{z_b}{y_b} \end{bmatrix} \tag{4}$$

The input linear r, g, b is first encoded as a nonlinear component by the EOTF and then mapped into tristimulus values. (X, Y, Z) by the LEDs. This model is based on the CIE xyY color space as it includes both chromaticity and luminance attributes, which facilitates direct quantification of the display characteristics of the terminal. With this model, the input image signal may be converted into an optical signal with terminal characteristics that can be received by the human eye or optical measuring instruments.

EOTF is an Electro-Optical Transfer function, which is utilized to encode and convert the input image electrical signals into optical output signals in the terminal color reproduction process, from the earliest linear coding to the nonlinear γ -EOTF to the Stevenson power law function[19] to PQ curves employed in HDR. The essence of this conversion is to encode the signal to improve the display's performance of bright and dark details, to achieve

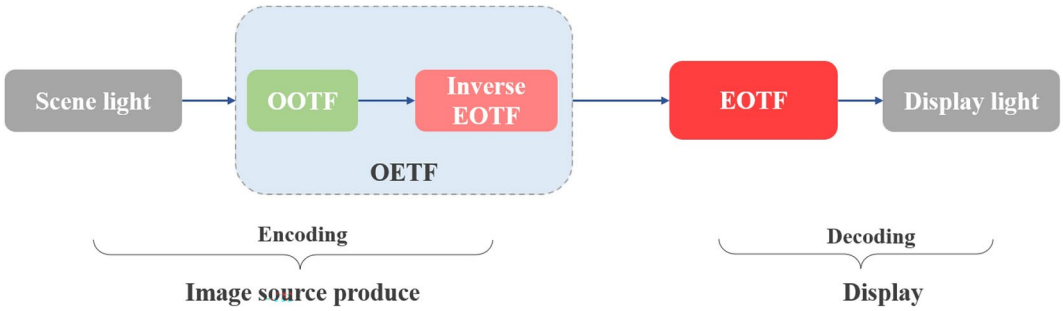

Figure 1. Schematic diagram of the process from image creation to display.

a wider range of colors and more realistic color performance while making it more in line with the human eye perception, which plays a significant role in the display process.

To reveal the general principles, this paper chooses the γ -EOTF, which has a concise description and is widely used, for analyzing and discussing. Substituting γ -EOTF into Eqs. (1)–(3), we can obtain the xyY model of the terminal.

$$x = \frac{X}{X+Y+Z} = \frac{\sum_{i=1}^{3} C_i \frac{x_i}{y_i} P_i{}^{\gamma}}{\sum_{i=1}^{3} C_i \frac{1}{y_i} P_i{}^{\gamma}} \tag{5}$$

$$y = \frac{X}{X+Y+Z} = \frac{\sum_{i=1}^{3} C_i P_i{}^{\gamma}}{\sum_{i=1}^{3} C_i \frac{1}{y_i} P_i{}^{\gamma}} \tag{6}$$

$$Y = \sum_{i=1}^{3} C_i P_i{}^{\gamma} \tag{7}$$

Where P_i and C_i respectively represent the three primary color signal components and white balance luminance ratio value, x_i and y_i represent the chromaticity parameter of the monochromatic color, subscript i, j can take the value of $1, 2, 3$, respectively, refer to r, g, b.

To ensure color consistency and accuracy when displayed on different devices, the vast majority of video and image content is now produced in adherence to the sRGB standard. Displays, as a medium for presenting images, are designed to show more gorgeous colors and usually possess a wide display gamut, such as LED displays. This contradiction leads to the fact that when WCGDs such as LEDs are fed into an image source of the sRGB standard without intervention, the input signal is processed in the terminal's color coding manner to ensure superior color performance, which results in oversaturated output colors.

As shown in Fig. 2, the original sRGB triangles are stretched into wide gamut triangles after the WCGD system, and the points in the gamut are also shifted to different degrees. This kind of shift is manifested as an increase in saturation and a deviation in hue, which will make the overall image appear more vibrant and provide a more powerful visual impression to the viewer. However, the shift will also bring a large color difference, resulting in the phenomenon of "over-saturation" of the images, some even beyond the human eye's conventional perception. For example, when displaying human skin, the skin color is excessively red, which significantly affects the viewing experience.

The cause of this problem is the mismatch between the image source and the display system, mainly the mismatch between the chromaticity attribute and the encoding manner. WCGDs possess a maximum physical gamut defined by the colorimetric parameters of the light-emitting chip, which can usually be converted into a smaller gamut within its physical gamut by gamut-limiting downward compatibility conversion to ensure better color reproduction.[20–23], However, the very high cost we spend on improving the color performance of the display, only a small part of it is utilized at last, which is more than worthwhile for the display terminal. The best solution is to seek a balance between maximizing the guaranteed gamut and visual effect optimization. This paper will make such an attempt.

Effect of EOTF on gamut properties

In this section, we will dissect the role of the encoding curve, EOTF, in the color oversaturation problem of WCGDs, and then analyze in depth and quantitatively the effect of the EOTF on the display terminal's color

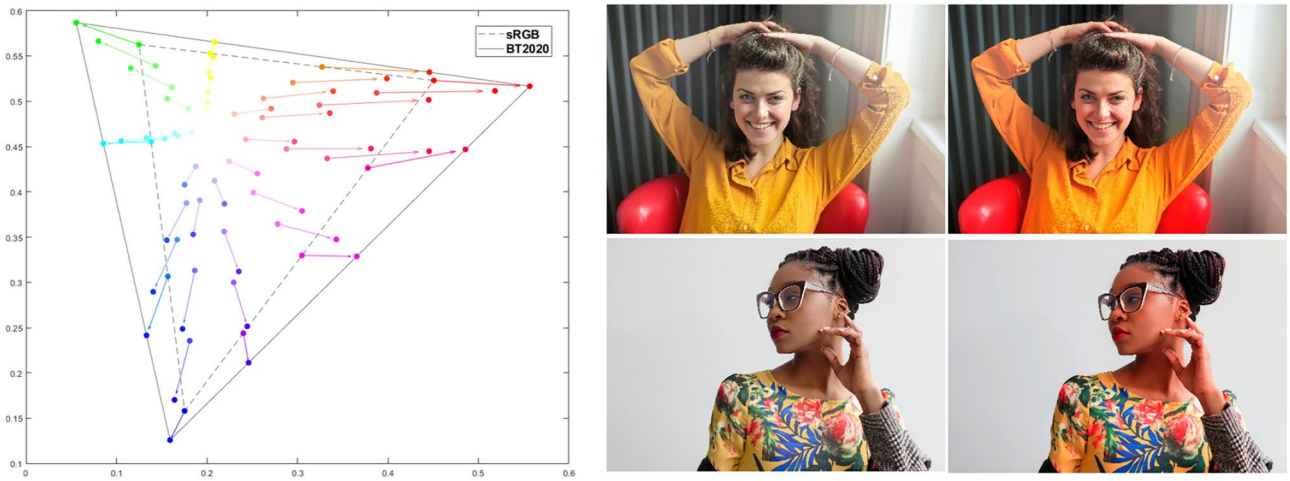

Figure 2. Schematic of WCGDs color oversaturation.

performance, mainly in terms of luminance and chromaticity. To facilitate the calculation, the most widely used gamma function is chosen for all the EOTF curves in this paper.

Effect of EOTF on color point distribution

According to the display model established in Part II, the EOTF output from a display system with linear r, g, b input is a set of dots. By encoding the r, g, b signals before inputting them into the display system, the output color's chromaticity coordinates will vary, and the distribution of color points in the 3D color space will be altered accordingly. Different encoding manners lead to different primary energy distributions, leading to different color point distributions, ultimately determining the color performance of the terminal. Figure 3 below shows the distribution of color points corresponding to different γ values in the sRGB standard in CIE xyY color space and relatively perception-uniform CIE Lab color space, respectively.

In the gamut triangle, the center tends to represent the white field, and the apex tends to represent the purer, more vibrant colors. It is not difficult to conclude from the figure that smaller γ values correspond to the denser distribution of color points in the center, i.e., more desaturated colors. As γ increases, the color dots gradually spread out across the gamut, becoming sparsely denser in the center and denser near the apex, and more evenly distributed across the uniform gamut. This aligns with the original purpose of the γ function being proposed, which is to fit more well with human eye perception. Human eye perception conforms to Weber's law:

$$\frac{\triangle L}{L} = k \tag{8}$$

This law describes the human eye's perception of luminance variations as proportional to luminance so that a person is much less sensitive to bright, unsaturated colors than to low-luminance, saturated ones. By encoding the color, the energy of the primary is more concentrated in the low-luminance interval, which implies a finer low-luminance coding. When the primaries are mixed for color reproduction, the finer encoding results in subtler color variations, and richer color hierarchies. The optimal encoding curve, or perceptual quantizer (PQ), is the one in which each gray-level encoding interval meets the minimum threshold for human eye perception.

Effect of EOTF on color reproduction in WCGDs

Further analysis of the color point position offsets in xyY color space, for any point (x, y, Y), there exists a vector $\sigma_\gamma(P_1, P_2, P_3)$=$(x_\gamma, y_\gamma, Y_\gamma)$ a direction in which the point changes with γ, where:

$$x_\gamma = \frac{\partial x}{\partial \gamma}(r, g, b), y_\gamma = \frac{\partial y}{\partial \gamma}(r, g, b), Y_\gamma = \frac{\partial Y}{\partial \gamma}(r, g, b) \tag{9}$$

Calculated by substituting the equation in Part I:

$$x_\gamma = \frac{sQ_x s^T}{s\mathrm{C}s^T}, y_\gamma = \frac{sQ_y s^T}{s\mathrm{C}s^T} \tag{10}$$

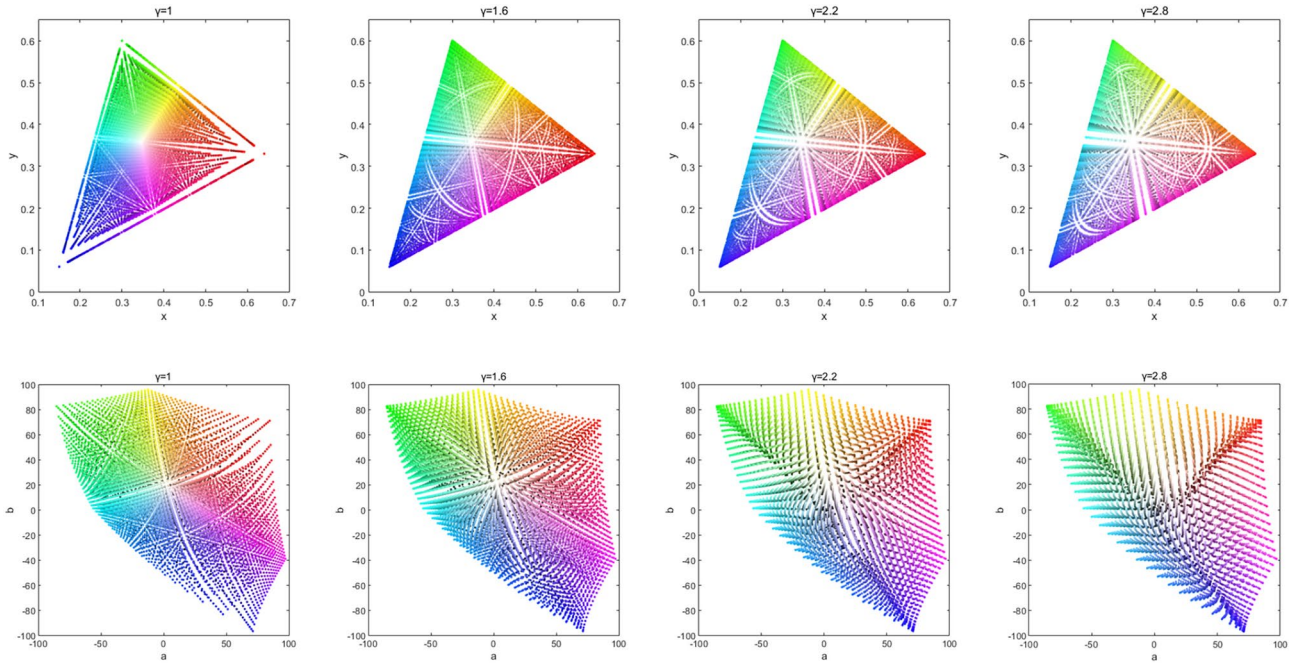

Figure 3. Schematic diagram of color point distribution with γ in sRGB.

$$Y_\gamma = C_Y s^T \tag{11}$$

where

$$s = [r^\gamma \quad g^\gamma \quad b^\gamma] \tag{12}$$

$$Qx = \begin{bmatrix} 0 & -\frac{C_1C_2}{y_r y_g}(x_g - x_r)lng & \frac{C_1C_3}{y_r y_b}(x_b - x_r)lnb \\ \frac{C_2C_1}{y_g y_r}(x_r - x_g)lnr & 0 & \frac{C_2C_3}{y_g y_b}(x_b - x_g)lnb \\ \frac{C_3C_1}{y_b y_r}(x_r - x_b)lnr & \frac{C_3C_2}{y_b y_g}(x_g - x_b)lng & 0 \end{bmatrix} \tag{13}$$

$$Qy = \begin{bmatrix} 0 & -\frac{C_1C_2}{y_r y_g}(y_g - y_r)lng & \frac{C_1C_3}{y_r y_b}(y_b - y_r)lnb \\ \frac{C_2C_1}{y_g y_r}(y_r - y_g)lnr & 0 & \frac{C_2C_3}{y_g y_b}(y_b - y_g)lnb \\ \frac{C_3C_1}{y_b y_r}(y_r - y_b)lnr & \frac{C_3C_2}{y_b y_g}(y_g - y_b)lng & 0 \end{bmatrix} \tag{14}$$

$$C_Y = [C_1 lnr \quad C_2 lng \quad C_3 lnb] \tag{15}$$

Simplifying the matrix yields:

$$x_\gamma = \frac{\sum_{i=1}^{3}\sum_{j=1}^{3} C_i C_j \frac{1}{y_i y_j}(x_j - x_i) P_i{}^\gamma P_j{}^\gamma \ln P_j}{\sum_{i=1}^{3}\sum_{j=1}^{3} C_i C_j P_i{}^\gamma P_j{}^\gamma} \tag{16}$$

$$y_\gamma = \frac{\sum_{i=1}^{3}\sum_{j=1}^{3} C_i C_j \frac{1}{y_i y_j}(y_j - y_i) P_i{}^\gamma P_j{}^\gamma \ln P_j}{\sum_{i=1}^{3}\sum_{j=1}^{3} C_i C_j P_i{}^\gamma P_j{}^\gamma} \tag{17}$$

$$Y_\gamma = \sum_{i=1}^{3} C_i P_i{}^\gamma \ln P_i \tag{18}$$

According to the results, the drift of luminance and chromaticity can be analyzed separately.

Effects on luminance

The display luminance is superimposed by the primaries' luminance. The primary luminance function curve satisfies the EOTF, i.e., the exponential curve, which increases exponentially with signal input.

$$Y_r = C_1 r^\gamma, Y_g = C_2 g^\gamma, Y_b = C_3 b^\gamma \tag{19}$$

According to the calculation above, the luminance variation vector Y_γ is:

$$Y_\gamma = \sum_{i=1}^{3} C_i P_i{}^\gamma \ln P_i \tag{20}$$

Primary color luminance variation curve and color points luminance variation vector field in gamut are graphed respectively as Fig. 4

For monochromatic luminance, the variation vector at a certain γ can also characterize the susceptibility of the display to fluctuations at a certain luminance. As shown in Fig. 4a, the blue component is the smallest and therefore has the smallest luminance fluctuation, while the green luminance fluctuates the most. In addition, γ mainly has a more pronounced effect on the luminance of the intermediate grayscale of the primary, and the luminance variation vector is essentially zero for colors with luminance components of 0 and 1. Moreover, as γ increases, the magnitude of the primaries' luminance variation vectors decreases. The peak of the vectors gradually moves to the higher grays, which may be explained by the fact that the encoding concentrates the energy to the lower grays increasing the affected gray levels. It becomes more apparent with γ grows.

When the primary colors are mixed, the extreme low-brightness and high-brightness color points are almost unaffected, so there is no variation in the vertex position of the gamut body. While the middle point by the influence of the primary luminance has shifted downward, the color points in the entire color gamut show a "downhill" trend.

Effects on chromaticity

The previous calculation yields the color coordinate shift-vector (x_γ, y_γ):

$$x_\gamma = \frac{\sum_{i=1}^{3}\sum_{j=1}^{3} C_i C_j \frac{1}{y_i y_j}(x_j - x_i) P_i{}^\gamma P_j{}^\gamma \ln P_j}{\sum_{i=1}^{3}\sum_{j=1}^{3} C_i C_j \frac{1}{y_i y_j} P_i{}^\gamma P_j{}^\gamma} \tag{21}$$

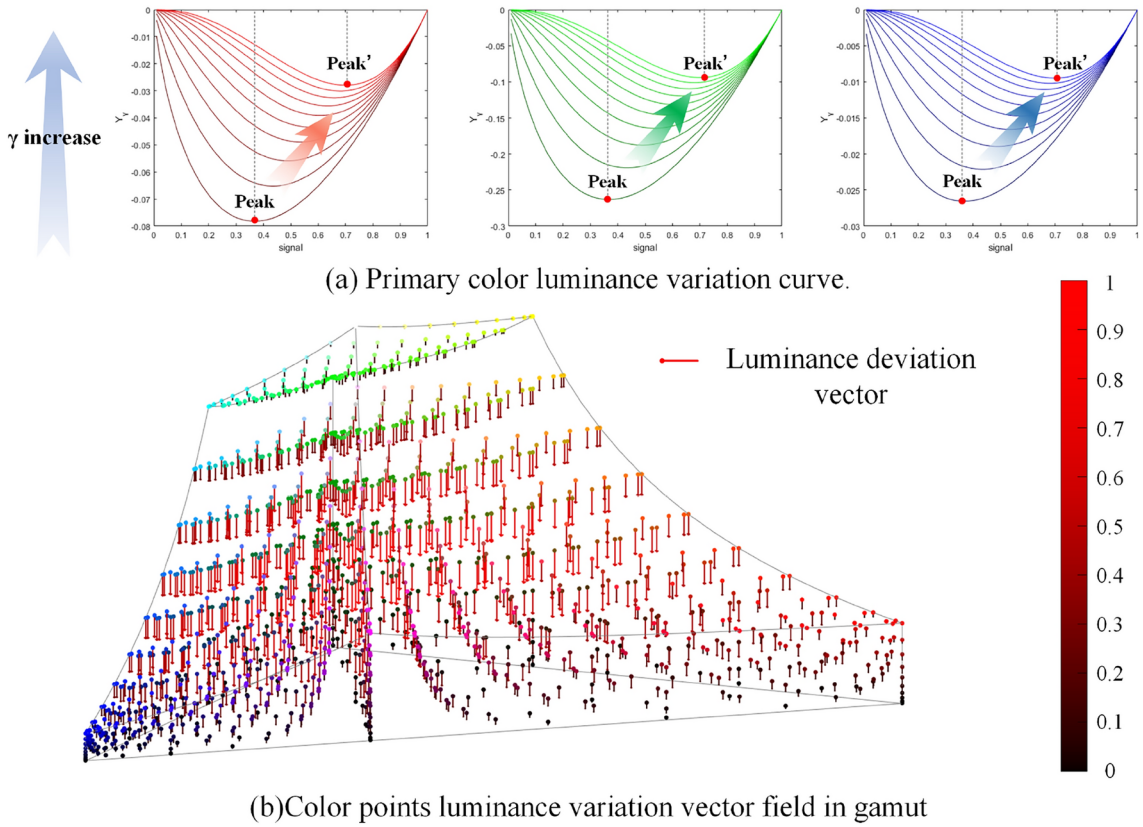

Figure 4. Variation of luminance with γ.

$$y_\gamma = \frac{\sum_{i=1}^{3}\sum_{j=1}^{3} C_i C_j \frac{1}{y_i y_j}\left(y_j - y_i\right) P_i{}^\gamma P_j{}^\gamma \ln P_j}{\sum_{i=1}^{3}\sum_{j=1}^{3} C_i C_j \frac{1}{y_i y_j} P_i{}^\gamma P_j{}^\gamma} \tag{22}$$

According to the Einstein summation convention, the expression can be abbreviated as:

$$x_\gamma = \frac{C_i C_j \frac{1}{y_i y_j} P_i{}^\gamma P_j{}^\gamma \widetilde{df}\left(x\right)}{C_i C_j \frac{1}{y_i y_j} P_i{}^\gamma P_j{}^\gamma}, \ \widetilde{df}\left(x\right) = \left(x_j - x_i\right) \ln P_j \tag{23}$$

$$y_\gamma = \frac{C_i C_j \frac{1}{y_i y_j} P_i{}^\gamma P_j{}^\gamma \widetilde{df}\left(x\right)}{C_i C_j \frac{1}{y_i y_j} P_i{}^\gamma P_j{}^\gamma}, \ \widetilde{df}\left(y\right) = \left(y_j - y_i\right) \ln P_j \tag{24}$$

where $\widetilde{df}$ is an offset factor that satisfies the logarithmic relationship with the independent variables range [0,1], which means that as the signal component approaches 1, the closer the offset factor nears 0, the smaller the coordinate offsets x_γ, y_γ are consequently, and vice versa as the signal component becomes smaller and approaches 0, the larger the coordinate offsets x_γ, y_γ are.

Geometrically speaking, smaller signal components generally produce color points distributed around the triangle vertex, so the color deviation in the triangle vertex region of the gamut will be more pronounced. And since the red primary color coordinates are relatively large, it will more likely lead to a larger offset factor, so the points in the red region (especially the points near the red vertice) have correspondingly greater coordinate deviations.

The chromaticity offset vectors within the gamut triangle are shown in Fig. 5. The vector color in the figure is proportional to the vector length, and it can be seen that the deviation trend is consistent with the results of the previous analysis, with an overall larger deviation at the vertices and the largest deviation in the red region. In addition, it is not difficult to recognize from the figure that all the vectors are pointing from the center to the vertices of the triangle, which means that almost all the colors tend to become more saturated. The color point deviation in the gamut leads the color to be saturated, and some of them with large deviations from the original color will show the phenomenon of oversaturation, which is what we know as the color oversaturation distortion problem of WCGDs.

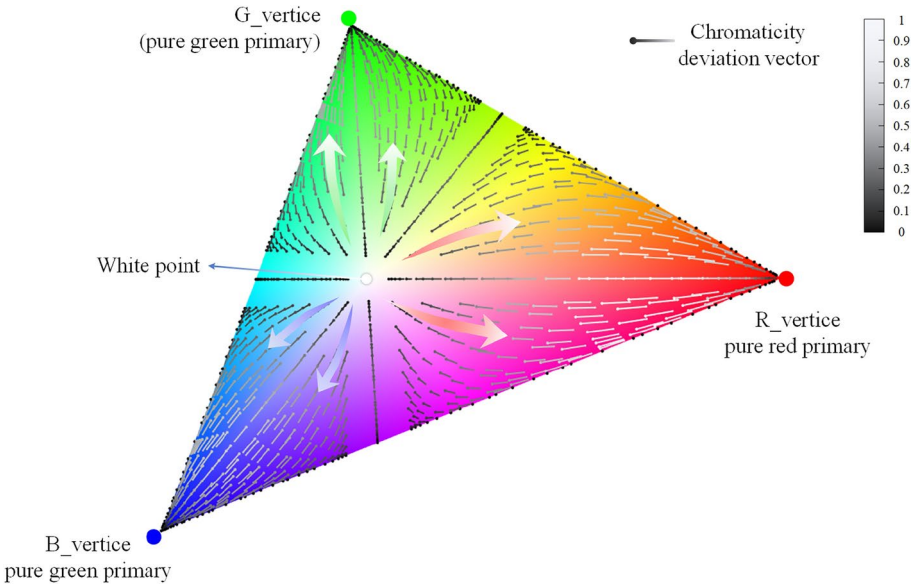

Figure 5. Chromaticity offset vectors within the gamut triangle.

Promising EOTF-based solutions

Based on the previous analysis and conclusion, the oversaturation problem of WCGDs is mainly attributed to the color point's deviation towards the triangle's vertex region under the encoding of EOTF (especially the red vertex region). Therefore, we can control the encoding manner of EOTF to make the color point deviate in the opposite direction to compensate for the original deviation of the color point, to achieve the purpose of adjusting the color accuracy.

Brief description of the experiment

Assuming that the display terminal satisfies the BT2020 gamut with $\gamma = 2.8$ and the input image source satisfies the sRGB standard with $gamma = 2.2$, the following two modification strategies are proposed:

Strategy 1: Modify the γ for all primary colors of the terminal from 2.8 to 2.2.

Strategy 2: To address the more severe red distortion, keep γ 2.8 for the blue and green primaries and modify the γ from 2.8 to 2.2 for the red primary only.

Experimental Data Sample: The three primary colors are input with normalized values from 0:0.01:1, forming 100^3 groups of color input drive samples.

According to ((5))–((7)) in the paper, the terminal output color parameters x, y, and Y for the sample values are calculated based on the EOTF curve specified by the control group. Then, 100^3 groups of color output values for Strategy 1 and Strategy 2 are obtained. The color differences between the two improvement strategies and the original values are then calculated, respectively.

To guarantee consistency with the human perception, the color difference indicator $\triangle uv$ in the uniform color space Luv is chosen as a metric to evaluate the color difference between the input video source and the display[24,25], and its value can be applied to evaluate the relative centrifugal degree of color deviation from the human eye.

First, the obtained output values are converted into the Luv color space. The formulas for calculating $L, u, andv$ are as follows:

$$u = \frac{4X}{X + 15Y + 3Z} = \frac{4x}{-2x + 12y + 3} \tag{25}$$

$$v = \frac{9Y}{X + 15Y + 3Z} = \frac{9y}{-2x + 12y + 3} \tag{26}$$

where x and y can be calculated using (1–3). Then,$\triangle uv$ can be calculated by the following Eq. (27):

$$\triangle uv = \sqrt{\triangle u^2 + \triangle v^2} \tag{27}$$

$$\triangle u = u_{WCGD} - u_{signal} \tag{28}$$

$$\triangle v = u_{WCGD} - u_{signal} \tag{29}$$

The 100^3 sets of color differences $\triangle uv$ between the output color values of the two strategies and the output color values based on the image display standards are calculated after the image signal is input into the display

	Origin		$\gamma = 2$	$\gamma = 2.1$	$\gamma = 2.2$	$\gamma = 2.3$	$\gamma = 2.4$	$\gamma = 2.5$	$\gamma = 2.6$	$\gamma = 2.7$
AVER	0.0611	s1	0.0378	0.0408	0.0438	0.0468	0.0498	0.0528	0.0528	0.0584
		s2	0.0456	0.0466	0.0480	0.0497	0.0517	0.0539	0.0562	0.0586
STD	0.0293	s1	0.0234	0.0240	0.0246	0.0253	0.0260	0.0268	0.0268	0.0284
		s2	0.0216	0.0215	0.0218	0.0224	0.0233	0.0245	0.0260	0.0275
VAR	0.0009	s1	0.0005	0.0006	0.0006	0.0006	0.0007	0.0007	0.0007	0.0008
		s2	0.0005	0.0005	0.0005	0.0005	0.0005	0.0006	0.0007	0.0008

Table 1. Color difference statistics of the proposed strategy.

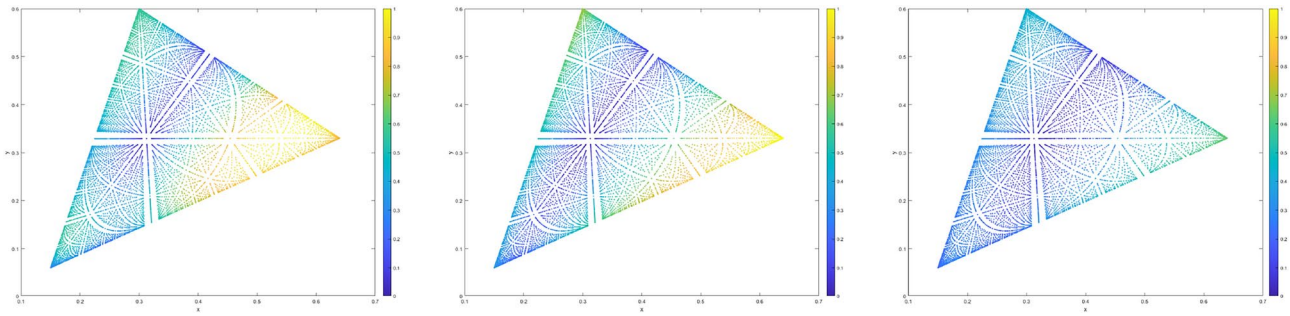

(a) Origin (b) Strategy 1 (c) Strategy 2

Figure 6. Diagram of color difference distribution in the gamut under three conditions.

system. Statistical analysis of the color difference data is then conducted to compare the effectiveness and superiority of the proposed solutions.

Data analysis

The statistical values of the color difference under the three conditions are as follows in Table 1. We compared the color differences of strategies in three dimensions: mean, variance, and standard deviation. The table shows that the mean and variance of the color difference are reduced to some extent by reducing the value of γ in Strategy 1 and Strategy 2. And reduction gradually decelerates as γ gets lower, demonstrating the effectiveness of the two strategies to some degree.

However, statistical values such as mean-variance can only show the overall trend of the data. According to the above analysis, the color difference of the three primary colors is inconsistent. Therefore, we divide the gamut triangle into three regions of red, green, and blue to further analyze the distribution of chromatic aberration in the gamut. The color point deviation $\triangle uv$ distribution in the gamut is illustrated separately under three circumstances in Fig. 6.

Firstly, it can be seen that the color deviation is mainly concentrated in the vertices of the triangle, and the red color deviation is larger than that of the other two, which is consistent with the previous analysis, and the human eye perception as well. Comparing the results of the two strategies with the original respectively, it can be seen that the yellow color at the three vertices in Fig.6b,c has shown signs of fading. However, Fig. 6b still maintains a similar red primary color distortion as the original one, while the relative errors of the primaries in Fig. 6c have been homogenized.

Further statistical analysis of the color difference data of the three primary colors, Chart of color difference statistics of R, G, and B, and the variation trend with γ is represented in Fig. 7.

The chart indicates that the green and blue color difference under both strategies remain relatively stable as γ decreases, while the red decreases significantly, and is equal to that of green and blue when $\gamma = 2.2$. In contrast, strategy 2, the solid part of the figure, presents a faster reduction of the red difference and a more stable stability of the green-blue difference than strategy 1, the dashed part of the figure. This means that Strategy 2 has an even superior capability of solving the oversaturation problem of WCGDs, making the color difference between the primaries relatively flat, thereby reducing the viewing discomfort caused by oversaturation and ensuring viewing comfort.

The simulation of the display effect of the image in the three situations is shown in Fig. 8. As can be seen from the picture, after EOTF modification, the person in the image no longer looks like an alcoholic, but has a more normal skin color. In contrast, the optimized image of Strategy 2 shows more vivid colors and higher overall contrast than the Strategy 1 image, which implies better detail performance ability and better color performance, proving the feasibility and effectiveness of the proposed scheme and the superiority of Strategy 2 in this paper.

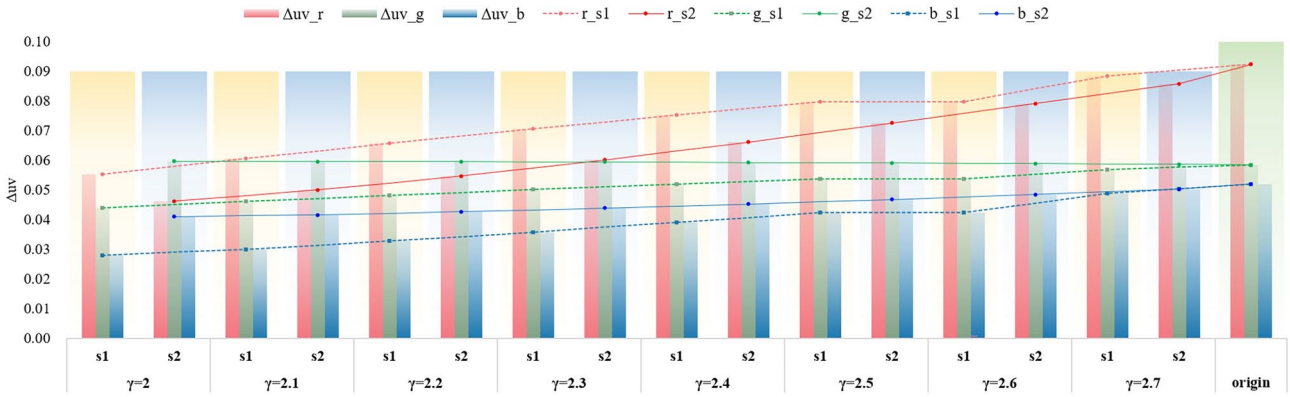

Figure 7. Chart of color difference statistics of R, G, and B and the variation trend with γ.

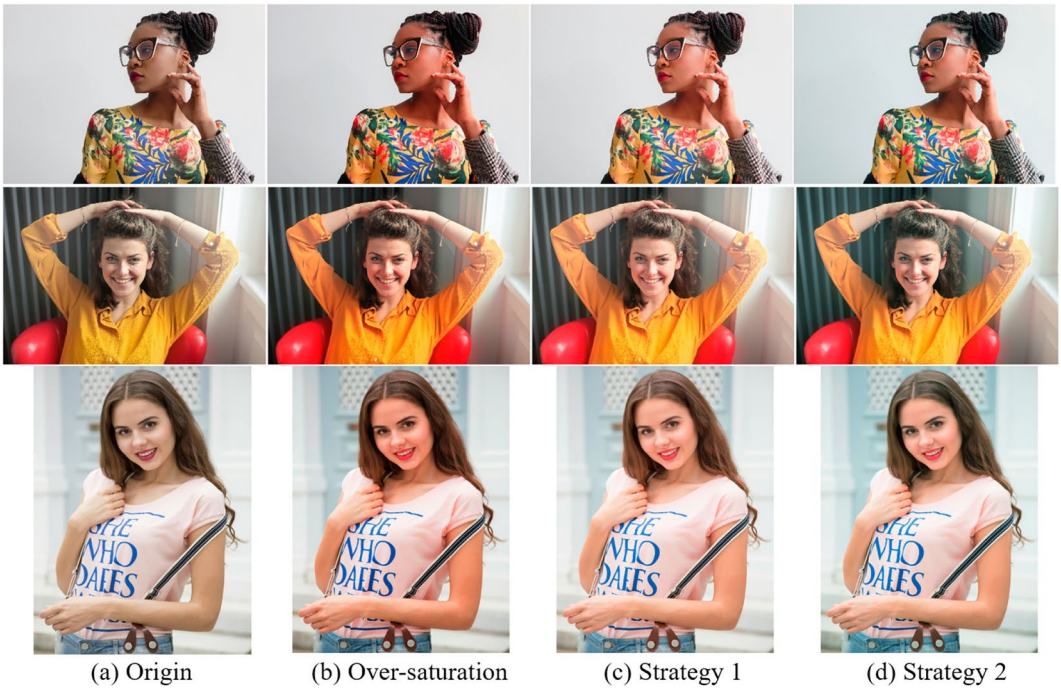

Figure 8. Simulation of the display effect of the image under three conditions.

Conclusion

Aiming at the display oversaturation problem of WCGDs, this paper establishes the vector variation field of luminance chromaticity drift with EOTF based on the 3-dimensional geometrical model of the display, and obtains the law of luminance chromaticity parameter drift with EOTF by analyzing the algebraic and geometrical significance of the vectors. According to the analysis conclusions, 2 correction strategies are proposed. Based on the chromatic aberration index, the performance of the two strategies in solving the color oversaturation problem of WCGDs is analyzed step by step from the whole to the partial, which verifies the idea that modifying the EOTF can improve the color gamut performance of WCGDs. By defining different EOTF curves for different primary, it is also possible to balance the chromatic deviation of the primaries in a targeted way, to achieve a display effect that is more in line with the human eye's vision.

However, this paper only equalizes the color difference of the primaries and does not consider the color deviation of the white field in the middle and low grayscale that may be caused by adopting different EOTFs. Modifying the display white balance parameters may also be a feasible way. In addition, only the simplest exponential form of EOTF has been considered in this paper. there are already many displays that use power functions and PQ curves as EOTFs, and these two forms of curves should be analyzed in the same way. In future research work, we hope to discuss the above issues in depth.

Data availability

The datasets used and/or analysed during the current study available from the corresponding author on reasonable request.

Received: 4 September 2024; Accepted: 14 November 2024
Published online: 21 November 2024

References

1. Masaoka, K. & Nishida, Y. Metric of color-space coverage for wide-gamut displays. *Opt. Express* **23**, 7802. https://doi.org/10.1364/OE.23.007802 (2015).
2. Wen, Z. et al. Color revolution: Toward ultra-wide color gamut displays. *J. Phys. D Appl. Phys.* **54**, 213002. https://doi.org/10.1088/1361-6463/abe43d (2021).
3. Inc, T. *LIFE* (Time Inc, 1950).
4. A Standard Default Color Space for the Internet - sRGB. https://www.w3.org/Graphics/Color/sRGB.
5. Lee, J., Vigier, T., Le Callet, P. & Lee, J.-S. Wide Color Gamut Image Content Characterization: Method, Evaluation, and Applications. *IEEE Trans. Multimedia* **23**, 3817–3827. https://doi.org/10.1109/TMM.2020.3032026 (2021).
6. Robertson, M. A., Borman, S. & Stevenson, R. L. Estimation-theoretic approach to dynamic range enhancement using multiple exposures. *J. Electron. Imaging* **12**, 219–228. https://doi.org/10.1117/1.1557695 (2003).
7. Kang, W. H., Chun Wan, G. & Tong, M. S. A Color Compensation Method for Three Primary-color LED Light Sources. In *2019 Photonics & Electromagnetics Research Symposium - Fall (PIERS - Fall)*, 741–744, https://doi.org/10.1109/PIERS-Fall48861.2019.9021816 (IEEE, Xiamen, China, 2019).
8. Babilon, S., Klabes, J., Myland, P. & Khanh, T. Q. Memory colors and the assessment of color quality in lighting applications. *Opt. Express* **29**, 28968. https://doi.org/10.1364/OE.426774 (2021).
9. Ko, M., Kwak, Y., Seo, G., Kim, J. & Moon, Y. Reducing the CIE colorimetric matching failure on wide color gamut displays. *Opt. Express* **31**, 5670. https://doi.org/10.1364/OE.480001 (2023).
10. Recommendation ITU-R BT.2100-2 (02/2018) Image parameter values for high dynamic range television for use in production and international programme exchange (2018).
11. ISO/TC 130. Adobe RGB (1998) Color Image Encoding (1998).
12. ITU-R. BT.2020 : Parameter values for ultra-high definition television systems for production and international programme exchange (2012).
13. Digital Cinema Initiatives,LLC. High Dynamic Range D-Cinema Addendum (2023).
14. Mann, S. & Ali, M. A. Chapter 1 - The Fundamental Basis of HDR: Comparametric Equations. In Dufaux, F., Le Callet, P., Mantiuk, R. K. & Mrak, M. (eds.) *High Dynamic Range Video*, 1–59, https://doi.org/10.1016/B978-0-08-100412-8.00001-2 (Academic Press, 2016).
15. Sharma, G. & Rodriguez-Pardo, C. E. Geometry of Multiprimary Display Colors I: Gamut and Color Control. *IEEE Access* **9**, 96573–96597. https://doi.org/10.1109/ACCESS.2021.3093395 (2021).
16. Smith, E., Heckaman, R. L., Lang, K., Penczek, J. & Bergquist, J. Measuring the color capability of modern display systems. *J. Soc. Inform. Display* **28**, 548–556. https://doi.org/10.1002/jsid.918 (2020).
17. Liu, F. et al. Effect of the spatial location of boundary on colour overflow in Gamut conversion. *Displays* **80**, 102556. https://doi.org/10.1016/j.displa.2023.102556 (2023).
18. Fairchild, M. Colorimetry. *In Color Appearance Models, chap.* **3**, 56–84. https://doi.org/10.1002/9781118653128.ch3 (John Wiley & Sons Ltd) (2013).
19. Stevens, S. S. Neural Events and the Psychophysical Law. *Science* **170**, 1043–1050. https://doi.org/10.1126/science.170.3962.1043 (1970).
20. Sikudova, E. et al. A Gamut-Mapping Framework for Color-Accurate Reproduction of HDR Images. *IEEE Comput. Graph. Appl.* **36**, 78–90. https://doi.org/10.1109/MCG.2015.116 (2016). arXiv:1711.08925.
21. Li, T. et al. Color gamut extension algorithm for various images based on laser display. *Opt. Express* **32**, 3891. https://doi.org/10.1364/OE.507868 (2024).
22. Xu, L., Zhao, B. & Luo, M. R. Colour gamut mapping between small and large colour gamuts: Part I gamut compression. *Opt. Express* **26**, 11481. https://doi.org/10.1364/OE.26.011481 (2018).
23. Candry, P., De Visschere, P. & Neyts, K. Color gamut volume and the maximum number of mutually discernible colors based on a Riemannian metric. *Opt. Express* **31**, 31124. https://doi.org/10.1364/OE.499593 (2023).
24. Safdar, M., Cui, G., Kim, Y. J. & Luo, M. R. Perceptually uniform color space for image signals including high dynamic range and wide gamut. *Opt. Express* **25**, 15131. https://doi.org/10.1364/OE.25.015131 (2017).
25. Costa, T., Gaudet, V., Vrscay, E. R. & Wang, Z. Perceptual Colour Difference Uniformity in High Dynamic Range and Wide Colour Gamut. In *2020 IEEE International Conference on Image Processing (ICIP)*, 161–165. https://doi.org/10.1109/ICIP40778.2020.9191176 (IEEE, Abu Dhabi, United Arab Emirates, 2020).

Acknowledgements

This work was supported by the Jilin Science and Technology Development Program - Major Science and Technology Project for Core Optoelectronic Devices and High-end Chips, Task No. 20210301001GX. Figures 2 and 8 was modified from Pixels (http://www.pexels.com/), licensed under a Creative Common zero(CC0) License (https://www.pexels.com/terms-of-service/).

Author contributions

F.L. conducted the experiments and wrote the main manuscript text. X.Z. provided the resources. Y.C. and Y.W. supervised this project. J.C. and D.H. finished the visualization. J.L., Z.X., and Y.C. finished the formal analysis. X.M. and H.C. did the validation. All authors reviewed the manuscript.

Declarations

Competing interests

The authors declare no competing interests

Additional information

Correspondence and requests for materials should be addressed to X.M.

Reprints and permissions information is available at www.nature.com/reprints.

Publisher's note Springer Nature remains neutral with regard to jurisdictional claims in published maps and institutional affiliations.